Contents lists available at SciVerse ScienceDirect

Chemical Engineering Research and Design

journal homepage: www.elsevier.com/locate/cherd

Experimental studies and numerical model validation of overflowing 2D foam to test flotation cell crowder designs

K.E. Cole, P.R. Brito-Parada, C. Xu[1], S.J. Neethling, J.J. Cilliers*

Rio Tinto Centre for Advanced Mineral Recovery, Froth and Foam Research Group, Department of Earth Science and Engineering, Imperial College London, South Kensington Campus, London SW7 2AZ, United Kingdom

ABSTRACT

A computational fluid dynamics model of froth motion has been developed to assess different flotation cell designs. This work presents an implementation of the model in a 2D case, to compare the simulated bubble velocity distribution and streamlines to an experimental foaming system. The model uses finite elements to solve Laplace's equation for a potential function from which the foam velocity can be obtained. It requires the air recovery, or the amount of air that overflows a flotation cell as unburst bubbles, as an input parameter to calculate the foam velocity distribution and bubble streamlines. The air recovery was obtained by image analysis from a vertical, overflowing monolayer of foam (2D) created in a Hele-Shaw column, which mimicked important flowing properties of flotation froths such as coalescence. Inserts were included in the foam column to represent potential crowder designs for industrial flotation cells. Three different designs were chosen to compare the effect of insert depth and shape, including rectangles and a triangle. The effect of the insert design on the overflowing foam is obvious from visual assessment of the bubble streamlines and velocity distribution, which were closely agreed by both the experiment and model.

Keywords: Froth flotation; Flotation bubbles; Image analysis; Computational fluid dynamics; Process optimisation

1. Introduction

Flotation machine design is constantly evolving to meet specific requirements of a particular industrial plant. The recent trend has been to increase the size of the flotation cell, which increases the froth volume. If this froth can only overflow at the vessel lip, the centre of the vessel becomes a large stagnant zone of froth which does not report to the concentrate (Zheng et al., 2004; Zheng and Knopjes, 2004). Therefore two different types of devices have been placed in the froth zone to improve mineral recovery: launders to increase the surface area for overflowing froth, and crowders to direct the froth flow. In this work, a model of foam flow has been developed that can predict the effect of insert design on overflowing foam, to give insight into the effect of crowder design on flotation performance.

The function of a crowder is to decrease the cross sectional area at the top of the froth to improve the froth removal dynamics in the flotation cell. The walls of a crowder provide a surface to direct froth toward the overflow launder. They reduce the amount of air required for operation, or alternatively increase the volume of overflowing froth for a particular air rate. Crowders usually extend from the impeller outwards and from the outer wall inwards, although they can be placed mid-cell directing towards the weir. A crowder design from a flotation cell at Rio Tinto's Northparkes mine is shown in Fig. 1, where the angled surface of the crowder directs the froth to overflow the weir on the right side of the image. Degner (1997) patented a crowder device designed to improve the removal of froth, reducing the amount of air needed to produce froth and thus the energy needed to power the cell rotor. Fuerstenau et al. (2007) described the effect of adding a conical crowder above the impeller hood to a Wemco 1+1 flotation machine, which increased the copper recovery by 18%. For a reasonably straight forward engineering solution, crowders can have a significant effect on flotation efficiency.

Computational fluid dynamics (CFD) is a powerful tool that can be exploited to optimise the performance of existing

* *Corresponding author*. Tel.: +44 20 75947145; fax: +44 20 7594 7444.
E-mail address: k.cole07@imperial.ac.uk (K.E. Cole).
Received 4 January 2012; Received in revised form 12 April 2012; Accepted 11 May 2012
[1] Present address: Institute of Computer Science and Technology, Peking University, China.
0263-8762/$ – see front matter
http://dx.doi.org/10.1016/j.cherd.2012.05.009

Fig. 1 – Photograph of a crowder device from a flotation cell at Rio Tinto's Northparkes mine.

systems and to develop new technology to maximise process efficiency. The flow of flotation froths can be modelled as a potential flow. Numerical models for flowing foams based on solving Laplace's equation for a stream function (Moys, 1984; Murphy et al., 1996; Neethling and Cilliers, 1999) have proven useful but present some limitations; in particular the fact that they are restricted to two-dimensional simulations.

Brito-Parada et al. (2012) developed a numerical model for the trajectory and velocity of a flowing foam that uses finite elements on unstructured meshes to solve Laplace's equation for a scalar function. The selection of a potential function over the stream function allowed the implementation of the model not only for two dimensions but, for the first time, also for three-dimensional cases.

As CFD models require the mathematical descriptions of a process to represent the phenomena as accurately as possible, the simulations must be validated with experimental data. This presents a problem for flotation modelling, as flotation froths are opaque and fragile meaning there is a lack of experimental methods to measure their internal behaviour. Cole (2010) developed an overflowing foam column to measure the internal bubble properties optically. Image analysis measurements were possible as the Hele-Shaw column contained a monolayer of bubbles, or quasi 2D foam. The two phase chemical system mimicked a flotation froth as it was designed to provide a dynamic, viscous and coalescing foam that overflowed and burst at the foam surface. Measurements of the bubble size distribution in this 2D column were used to validate a coalescence model in Tong et al. (2011), which combined a liquid drainage model and a population balance model to predict the bubble size distribution over the height of the foam.

Image analysis methods can also be used to measure the bubble velocity and average flow streamlines in the 2D column, presenting a useful opportunity to validate the model of foam flow developed by Brito-Parada et al. (2012). The overflowing foam behaviour can be quantified in terms of the air recovery, or amount of air that overflows as unburst bubbles. This is important for the foam flow model which cannot yet predict the air recovery, making it a key parameter in determining the bubble velocity profile. As recent studies have highlighted a link between the air recovery and performance of a flotation cell (Ventura-Medina et al., 2003; Barbian et al., 2007), the inclusion of air recovery in this analysis allows direct comparison to a flotation cell.

2. Model for froth motion

By considering irrotationality and incompressibility of the foam, both valid assumptions as discussed by Neethling and Cilliers (2003), Laplace's equation is solved in the model by Brito-Parada et al. (2012) for the potential field ϕ:

$$\nabla^2\phi = 0. \tag{1}$$

The boundary conditions for the model are based on the geometry of the flotation cell, the air flowrate to the tank Q_a, and also on the air recovery α, an important variable in froth flotation. Assuming that the flux through the boundaries is uniform:

- At the solid walls:

$$\nabla\phi \cdot \mathbf{n} = 0. \tag{2}$$

- At the liquid/foam interface, A_I:

$$\nabla\phi \cdot \mathbf{n} = -\frac{Q_a}{A_I}. \tag{3}$$

- At the outflow, A_O:

$$\nabla\phi \cdot \mathbf{n} = \frac{Q_a\alpha}{A_O}. \tag{4}$$

- At the top surface of the foam, A_S:

$$\nabla\phi \cdot \mathbf{n} = \frac{Q_a(1-\alpha)}{A_S}. \tag{5}$$

As can be seen from the boundary conditions, air recovery is an important input for the model. Air recovery has been demonstrated to play a key role on the performance of flotation systems (Barbian et al., 2007), and it has been found not only that a peak in air recovery exists in industrial flotation froths but also corresponds to the air rate at which the highest overall mineral recovery is obtained (Hadler and Cilliers, 2009).

The numerical model for foam velocity of Brito-Parada et al. (2012) was implemented in Fluidity (AMCG, 2011), the finite element code which provides the computational framework for the model. In particular, the use of adaptive anisotropic meshes provides a means of capturing strong gradients of the flow and therefore is ideal for highly detailed simulations.

Experiments of flowing foams with inserts at the top, resembling crowders in flotation cells, can be used to study the effect these have on the flow. They also provide case studies to assess the capability of the numerical model to predict foam flow patterns and the velocity distribution of the flowing foam.

3. Experimental method

A Hele-Shaw type column is composed of two vertical parallel plates, with a narrow space in between. In this work, a plate separation of 5 mm was used to create a foam with only one layer of bubbles between two Perspex plates of size 400 mm × 400 mm. Two internal weirs with outwardly angled tops created a foaming space and an area for the liquid from the overflowing foam to recycle, as shown in Fig. 2. Air was supplied at the base of the column at a rate of 2.5 l/min.

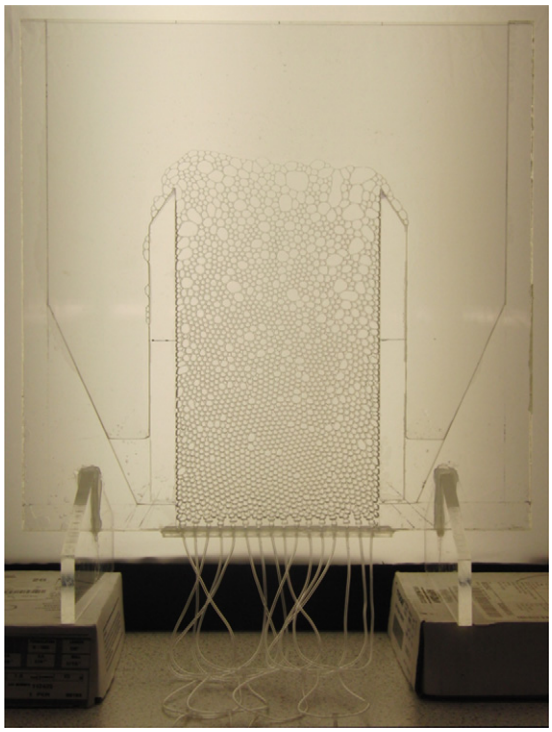

Fig. 2 – Photograph of the overflowing foam column.

The surfactant methyl isobutyl carbinol (MIBC) was used to create a foam that not only burst at the surface with internal coalescence, but also that overflowed and broke down rapidly after overflowing. Xanthan gum was added to the MIBC foaming solution to increase the foam viscosity to a level of 10–15 cP as suggested by Ata et al. (2006) to mimic flotation froths.

A superficial gas velocity, J_g, of 5.2 cm/s was required to provide an overflowing foam in the small foam column with 60 ml of aqueous solution. The initial bubble size was very uniform around a mean of 10.5 mm^2 and evenly distributed across the column width. The foam achieved steady state after 20 min. All experiments were performed at similar ambient temperature and humidity.

Different inserts were positioned in the foaming space of the column to change the foam flow analogous to industrial crowders. A rectangular insert of width 80 mm was positioned at two depths of 31 mm and 125 mm (defined below the level of the weir), and a triangular insert of width 60 mm and apex angle 54° was positioned at a depth of 60 mm.

The foam column was placed in front of a strong diffuse light source to increase the shadow of the foam Plateau borders visible to a digital camera. High speed videos of the flowing foam were captured at a rate of 210 frames per second and pixel resolution of 480 × 360. This camera was also used to capture a high speed, high resolution sequence at a rate of 40 frames per second. The images were prepared and analysed with the image processing software ImageJ (Rasband, 2009).

An image sequence was obtained from a high speed video of the overflowing bubble profile, where the bubble centres were approximately aligned vertically as they overflowed the weir. Two measurements were performed for each bubble with image analysis: the vertical separation between the bubble centre and the bubble centre immediately below (Δh_i), and the horizontal velocity ($v_{h,i}$) over a number of frames. For the bubble immediately above the weir, the vertical distance of the bubble centre to the weir (h_0) and its horizontal velocity over the weir ($v_{h,0}$) were also measured. The air recovery was therefore calculated as:

$$\alpha = \frac{l}{Q_a}\left(v_{h,0}h_0 + \sum_{i=1}^{n} v_{h,i}\Delta h_i\right), \quad (6)$$

where n is the total number of bubbles in each measurement and l is the length of the lip. In this work, a symmetrical overflowing profile was assumed, and the measurement from one side of the column was doubled to provide the resulting air recovery.

An algorithm was written in Matlab to calculate the velocity of a sample of bubbles between two consecutive high resolution images. The distance moved by each bubble between these frames was small compared to the average bubble size. For each bubble in the first frame, the algorithm searched for the nearest bubble in the second frame by comparing the bubble centre co-ordinates. This method of tracking the movement of bubbles within the foam is analogous to the particle tracking velocimetry (PTV) algorithm described in Bown et al. (2006), where it was shown that the size of the particles being tracked and their displacement between subsequent images is a critical factor to achieve adequate spatial resolution. For these techniques to yield accurate results, it is essential that the flow conditions are such that the nearest neighbour items (e.g. particles, bubbles) in subsequent images are likely to be the same items being tracked. Therefore in these experiments, image sequences were selected where minimal coalescence occurred, and any bubbles coalescing were ignored by the algorithm. Coarsening effects were also minimal, as air was used as the gaseous phase.

The resulting distance between bubble centres in each frame was divided by the time separation between frames, 0.025 s, to calculate individual bubble velocities. By interpolating the bubble velocity data into two dimensional arrays, the average bubble speed distribution was plotted as a map. A grid was defined with intervals at 10 mm over the column foaming space. Values of horizontal and vertical velocity were averaged for any bubble centres occurring within each element. The mean of three velocity measurements was plotted as streamlines, despite actually being average bubble tracks. This enabled direct comparison to the results of the model of foam motion.

4. Results and discussion

The air recovery was measured without inserts, then with the three different designs, as shown in Table 1. The error corresponds to the standard deviation in the mean air recovery for each insert. The standard deviation of the mean air recovery was often large, due to a high range of variability in the measurements of the air recovery. However, within the limits of the standard deviation, the inclusion of the inserts in the overflowing foam column led to an increase in the air recovery.

Table 1 – Air recovery with different insert design in the overflowing foam column.

Insert	Air recovery	Error
No insert	0.29	0.04
Rectangular (80 mm × 31 mm)	0.62	0.21
Rectangular (80 mm × 125 mm)	0.68	0.12
Triangular (60 mm × 60 mm)	0.68	0.11

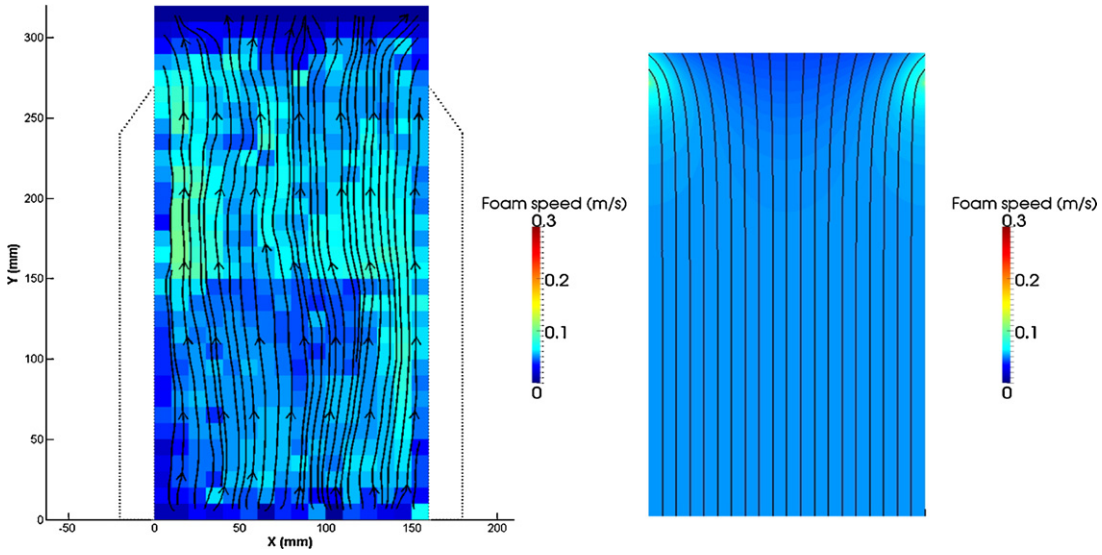

Fig. 3 – Plot showing the experimental (left) and simulated (right) average bubble speed distribution and flow streamlines without insert.

The experimental and simulated average bubble speed distributions and flow streamlines for a superficial gas velocity of 5.2 cm/s are shown in Fig. 3. The experimental and simulated streamlines are similar: all are directed upwards, with any significant horizontal deviation occurring above the weir. The simulation predicts a V-shaped section of slower bubbles at the foam surface, in agreement with the experimental speed distribution.

The experimental and simulated average bubble speed distributions and flow streamlines for the overflowing foam column with the 80 mm × 31 mm insert are shown in Fig. 4. The presence of the insert increased the average bubble speed over the total area of the column. Maximum speeds occurred around the corners of the insert and over the weir. The air recovery of this system was approximately double the value of the column with no insert; 0.62 compared to 0.29. This increase in air recovery can be attributed to the large horizontal deviations in the streamlines around the corners of the insert. Bubbles which collided with the base of the insert decelerated upon impact, but those which were deviated around the insert accelerated to at least twice their speed. The streamlines straightened in between the insert and the weir before overflowing (as a reflection of the insert shape), which could be a potential cause of the few streamlines which did not overflow.

The simulated average bubble speed distribution generally agrees with the experimental equivalent. The bubble streamlines were similar in both experiment and simulation, including the straightening effect of the rectangular insert shape. The experimental and simulated average bubble speed distributions also agreed on the zone of low bubble speeds near the base of the insert, and the high speed areas above the insert.

The average bubble speed distribution and flow streamlines in the overflowing foam column with insert 80 mm × 125 mm are shown in Fig. 5. As with the other rectangular insert, the average bubble speed was increased everywhere in the foaming column with the inclusion of the insert. The deviation in the streamlines around the corners of the insert was not as pronounced as observed previously for the other rectangular insert, however the area of low speed directly under the insert was still present. The increased depth of the rectangular insert reduced the area of the foaming space by 25%, which had a squeezing effect on the bubbles and caused rapid acceleration towards the weir. The high value of air recovery, 0.68, is a result of the high bubble speeds in between the weir and insert, despite the apparent low number of streamlines directed to overflow the weir.

The average bubble speed in between the insert and the weir was underestimated by the simulation, whereas the simulation did predict the higher bubble speed near the corners of the insert. In the simulation, the area of lower speed under the insert was much larger than measured experimentally. The high degree of deviation in the streamlines above the weir is evident in the simulation, but was not measured experimentally. It is likely that these streamlines did in fact exist in the overflowing column to contribute to the increase in air recovery.

The average bubble speed distribution and flow streamlines in the overflowing foam column with the triangular insert are shown in Fig. 6. The presence of the insert also increased the average bubble speed distribution, however the area of lower speed underneath the insert was much smaller at the triangle apex than at the rectangular insert bases. The triangular insert deviated the streamlines more gradually towards the weir, with less compression of streamlines and acceleration than observed with the rectangular inserts. The additional bubble path length in overflowing streamlines introduced by the insert is shortest for the triangular insert. This may be the reason why the triangular insert led to a similar air recovery as the rectangular inserts, despite causing less bubble acceleration in between the insert and weir.

In the experimental data, the average bubble speed was higher in the base of the column, with minimal acceleration above the insert. The acceleration through the height of the column was much more pronounced in the simulation. The simulated and experimental streamlines were very similar; especially in the degree of deviation in the overflowing streamlines.

It would be logical to expect the air recovery to stay constant with insert width, as increasing the insert width would be continually reducing the area at the top of the column through which the foam flows. However, the magnitude of the increase in air recovery due to the inclusion of the inserts

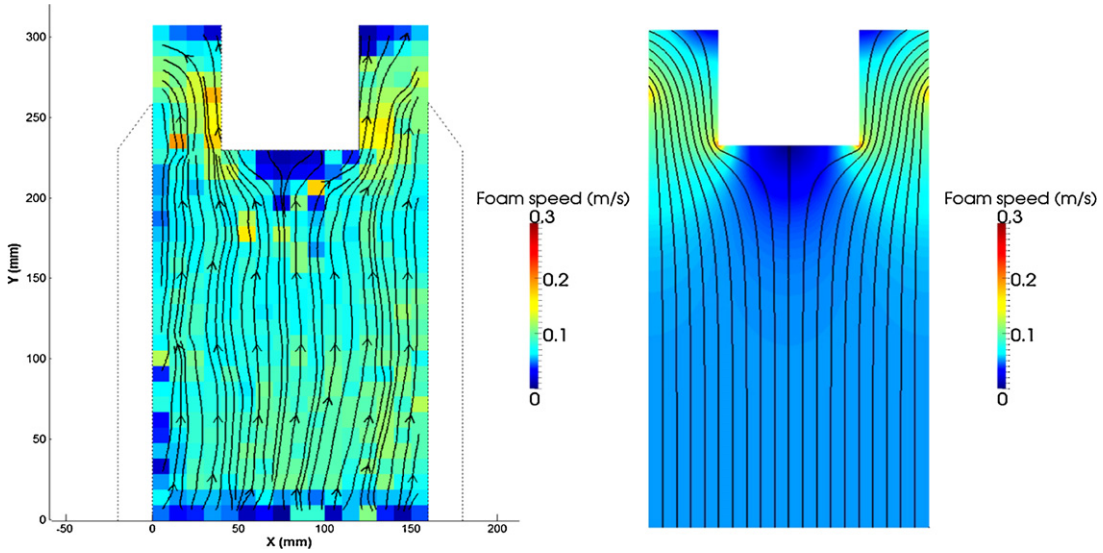

Fig. 4 – Plot showing the experimental (left) and simulated (right) average bubble speed distribution and flow streamlines with the rectangular 80 mm x 31 mm insert.

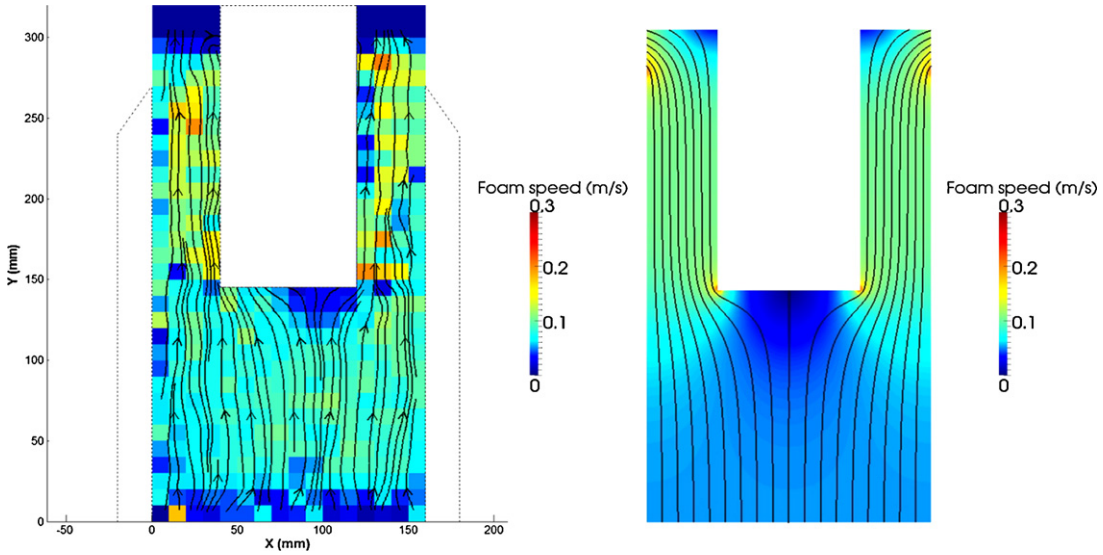

Fig. 5 – Plot showing the experimental (left) and simulated (right) average bubble speed distribution and flow streamlines with the rectangular 80 mm x 125 mm insert.

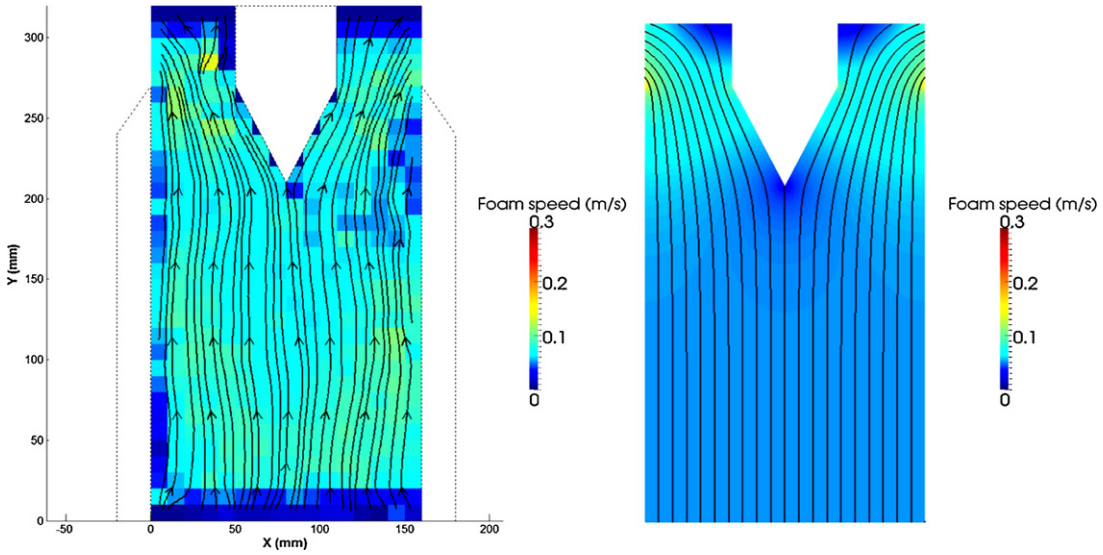

Fig. 6 – Plot showing the experimental (left) and simulated (right) average bubble speed distribution and flow streamlines with the triangular 60 mm x 60 mm insert.

was similar for both the rectangular and triangular designs, despite a difference in width of 20 mm. This implies that the insert shape is an important factor in determining the air recovery.

The compression of streamlines, or squeezing effect, leading to bubble acceleration may increase the probability of bubble collisions and thus an increase in coalescence. This behaviour associated with the rectangular inserts would not be desirable in an industrial flotation cell, implying that the triangular insert was the best insert investigated in this work. If the triangular shape was extended above the level of the weir (i.e. the rectangular portion of the insert replaced), it is likely that the air recovery would be increased further as more streamlines would be directed to overflow.

Overall, the close agreement between the model of foam flow and the experimental measurements mean that the model can be used to predict the optimum insert design for an overflowing foam column of this design.

5. Conclusion

A model of froth flow has been developed to predict the behaviour of different flotation cell designs. To validate the model with experimental data, simulations of a 2D overflowing foam column with different inserts were carried out. The inserts mimic the effects of different crowder designs, with important implications for flotation cell evaluation and design.

In the experimental data, three different insert designs increased the air recovery of the overflowing foam column by a similar amount; at least double. However, the increase in air recovery was attributed to three different effects: a rapid change in flow direction near the foam surface increasing the speed of the foam flow; a squeezing effect in between the weir and insert due to a significant decrease in foam volume, and a gradual change in flow direction with less acceleration in between the insert and weir.

Overall, the simulations closely predicted the average bubble speed and streamline behaviour observed in the experimental overflowing foam column for different inserts. As the froth motion model has been validated for 2D flowing foams, with an extension into 3D, it can be used to assess new crowder designs on industrial flotation cells.

References

Ata, S., Pigram, S., Jameson, G.J., 2006. Tracking of particles in the froth phase: an experimental technique. Miner. Eng. 19, 824–830.

AMCG, 2011. Fluidity Manual, Version 4.1. Applied Modelling and Computation Group. Department of Earth Science and Engineering, Imperial College London.

Barbian, N., Cilliers, J.J., Morar, S.H., Bradshaw, D.J., 2007. Froth imaging, air recovery and bubble loading to describe flotation bank performance. Int. J. Miner. Process. 84 (1–4), 81–88.

Bown, M.R., MacInnes, J.M., Allen, R.W.K., Zimmerman, W.B.J., 2006. Three-dimensional, three-component velocity measurements using stereoscopic micro-PIV and PTV. Meas. Sci. Technol. 17, 2175–2185.

Brito-Parada, P.R., Kramer, S.C., Wilson, C.R., Pain, C.C., Neethling, S.J., Cilliers, 2012. A finite element formulation to model the flow of flotation foams. Chem. Eng. Sci. 69 (1), 279–286.

Cole, K.E., 2010. Bubble size, coalescence and particle motion in flowing foams. Ph.D. Thesis. Imperial College London.

Degner, V.R., 1997. Flotation cell crowder device. United States Patent and Trademark Office, US Patent 5,611,917 (Mar.).

Fuerstenau, M.C., Jameson, G.J., Yoon, R.-H., 2007. Froth Flotation: A Century of Innovation. Society for Mining, Metallurgy and Exploration, Inc., Colorado.

Hadler, K., Cilliers, J.J., 2009. The relationship between the peak in air recovery and flotation bank performance. Miner. Eng. 22 (5), 451–455.

Moys, M.H., 1984. Residence time distributions and mass transport in the froth phase of the flotation process. Int. J. Miner. Process. 13 (2), 117–142.

Murphy, D.G., Zimmerman, W., Woodburn, E.T., 1996. Kinematic model of bubble motion in a flotation froth. Powder Technol. 87 (1), 3–12.

Neethling, S.J., Cilliers, J.J., 1999. A visual kinematic model of flowing foams incorporating coalescence. Powder Technol. 101 (3), 249–256.

Neethling, S.J., Cilliers, J.J., 2003. Modelling flotation froths. Int. J. Miner. Process. 72 (1–4), 267–287.

Rasband, W.S., 2009. ImageJ. U.S. National Institutes of Health, Bethesda, MD, USA. [Online]. Available from: http://rsb.info.nih.gov/ij/ (accessed 04.12.09).

Tong, M., Cole, K.E., Neethling, S.J., 2011. Drainage and stability of 2D foams: foam behaviour in vertical Hele-Shaw cells. Colloids Surf., A 382 (1–3), 42–49.

Ventura-Medina, E., Barbian, N., Cilliers, J.J., 2003. Froth stability and flotation performance. In: XXII International Minerals Processing Congress, Cape Town, South Africa, 28 September–3 October 2003.

Zheng, X., Knopjes, L., 2004. Modelling of froth transportation in industrial flotation cells: part II. Modelling of froth transportation in an Outokumpu tank flotation cell at the Anglo Platinum Bafokeng-Rasimone Platinum Mine (BRPM) concentrator. Miner. Eng. 17, 989–1000.

Zheng, X., Franzidis, J.P., Manlapig, E., 2004. Modelling of froth transportation in industrial flotation cells: part I. Development of froth transportation models for attached particles. Miner. Eng. 17, 981–988.